International Journal of Computer Science and Information Technology
ISSN: 3005-9682 (Print), ISSN: 3005-7140 (Online) | Volume 3, Number 3, Year 2024
DOI: https://doi.org/10.62051/ijcsit.v3n3.29
Journal homepage: https://wepub.org/index.php/IJCSIT/index

Study on the Binary Resistive Modulation technique of the PLCC Technology in the Streetlamp Monitoring System

Jiang Tao [1, 3, *], Md Gapar Md Johar [2], Jacquline Tham [3]

[1] College of Electronic Engineering, Anhui Xinhua University, Hefei, China

[2] Software Engineering and Digital Innovation Center, Management & Science University, Shah Alam, Malaysia

[3] Postgraduate Centre, Management & Science University, Shah Alam, Malaysia

*Corresponding Author: Jiang Tao

ABSTRACT

As a low-cost, open, and extensively covered communication technology, power line carrier communication (PLCC) technology has been applied to the streetlamp monitoring system to improve management quality. However, existing PLCC technologies face two problems: i. Significant signal attenuation on the power line, which limits transmission distance; ii. Inability to transmit signals across transformers due to the signal-blocking effect of transformers. To solve the problems, this paper introduces the resistive modulation technique into PLCC technology. Experiments show that the designed communication system has two advantages: i. It can transmit signals over long distances, as signal attenuation on the power line is suppressed; ii. It can transmit signals across the transformer as resistive signals are amplified when they are transmitted across the transformer.

KEYWORDS

Resistive modulation; PLCC technology; Signal attenuation; Transformer

1. INTRODUCTION

With the development of urbanization and technology, street lamps with a smart monitoring system have become an important part of smart cities [1]. A perfect streetlamp monitoring system can improve the quality of management effectively, which can save more energy without reducing safety [2]. And the trend of modern streetlamp monitoring systems development is to monitor street lamps remotely and intelligently [3]. In order to monitor street lamps in time, it is necessary to build a communication system between the monitor and the street lamps [4].

There are three common communication methods to build a streetlamp monitoring network: i. Radio frequency technology, such as Wireless Fidelity (WIFI), Global System for Mobile Communications (GSM), ZigBee, etc. [5]. These technologies require building their own network with limited coverage [6, 7]; ii. Rewiring. This method is suitable for new streetlamp monitoring systems, but involves high costs and complexity [8]; iii. Power Line Carrier Communication (PLCC) technology. PLCC technology transmits signals over existing power lines [9].

Compared with other methods, PLCC technology offers two main advantages: i. low cost. As a wired communication method without additional investment in new lines [10], PLCC is significantly more cost-effective than other wired communication methods over the same distance [4]. ii. Extensive coverage. As a physical network with the highest occupancy rate in the current society [11], power lines connect all the street lamps, enabling PLCC technology to connect every street lamp too [12].

Currently, PLCC technology is widely adopted in intelligent streetlamp monitoring systems [3]. In 2018, Yue Jiaqi et al. designed a streetlamp monitoring system based on PLCC technology [13]. This system monitors the street lamps by the PLCC between the streetlamp controller and the concentrator, handling tasks such as detecting damage, turning street lamps on or off, and adjusting input voltage, etc. However, the transmission distance is limited due to increased signal attenuation over longer distances [8]. In 2019, Shen Dan et al. designed an accurate streetlamp monitoring system based on PLCC technology [12]. Tests showed that this system could monitor each street lamp accurately. However, the system could only work on one side of the transformer due to the signal-blocking effect of the transformer, and the signal period of about 800 ms indicated a low communication rate [12].

As discussed above, this paper applies the PLCC technology to the streetlamp monitoring system. But there are 2 problems:

i. Signal attenuation in the power line. When the voltage signals are transmitted through power lines, signal attenuation occurs [14], which increases with transmission distance [8]. Currently, communication distance is typically less than 1 kilometer (km) [8, 15].

ii. Signal-blocking effect in the transformer. Power carrier signals can only be transmitted on one side of a transformer, as the transformer significantly reduces these signals. When signals are transmitted across a transformer, the attenuation can reach up to 100 decibels (dB) [10].

2. RESISTIVE MODULATION TECHNIQUE OF PLCC TECHNOLOGY

To address the above-mentioned problems, the resistive modulation technique is introduced into the PLCC technology, which transmits information via signals modulated by changing resistance.

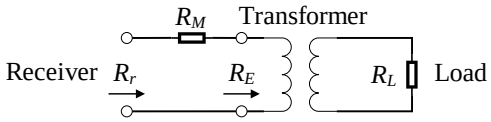

Figure 1. The framework for the resistively modulated PLCC technology

As shown in Fig. 1, the equivalent resistance perceived by the receiver (R_r) will change as the resistance of the load (R_L) changes according to Eq. 1 [16].

$$\Delta R_E = \left(\frac{N_E}{N_L}\right)^2 \Delta R_L \tag{1}$$

Where ΔR_L represents the resistance change on the transformer's secondary side, ΔR_E represents the corresponding change in equivalent resistance from the primary side to the secondary side, N_E is the number of turns on the primary side, and N_L is the number of turns on the secondary side. The resistive modulation technique has two advantages:

i. It can transmit signals across the transformer. Eq. 1 shows that the attenuation of resistive signals transmitted across the transformer can be adjusted by the winding ratio of the transformer N_E/N_L.

ii. It can improve the communication distance of the system by eliminating signal attenuation in the power line. This is illustrated by Eq. 2 according to [17].

$$\Delta R_r = \Delta R_E + \Delta R_M \tag{2}$$

Where ΔR_E represents the change in equivalent resistance from the primary side to the secondary side, ΔR_r represents the change in the equivalent receiving resistance, and ΔR_M represents the change in the residual resistance of the power line, which can be ignored as shown in Eq. 3.

$$\Delta R_M = 0 \tag{3}$$

When resistive signals are transmitted, they remain constant despite changes in transmission distance, as described by Eq. 4.

$$\Delta R_r = \Delta R_E \tag{4}$$

3. EXPERIMENTAL PROCEDURE

3.1. Experimental Environment Setup

MATLAB is a powerful tool for simulating PLCC technology, supporting the research and development of complex signal transmission and data communication systems within power grids [18]. Therefore, MATLAB is utilized for data analysis and simulation in the experiments.

It is necessary to set parameters to establish a model for the experimental PLCC system. As shown in Fig. 2, In this model, the transformer's winding ratio is N_E/N_L, Voltage Sensor1 is used to measure the voltage (u_M) across the measuring resistance (R_M), and Voltage Sensor2 measures the source voltage (u_S) with a bleeder circuit. Both sensors are the same type of Analog-to-Digital Converter (ADC) chip. And the phase difference (ϕ) can be obtained by ϕ_{uS} - ϕ_{uM}, where ϕ_{uS} is the initial phase of u_S, ϕ_{uM} is the initial phase of u_M. Additionally, there are M street lamps (R_{SLm}, m = 1, 2, …, M) with corresponding digital resistors (R_{Dm}, m = 1, 2, …, M) on the secondary side of the transformer, and each lamp can transmit signals by adjusting its corresponding digital resistor.

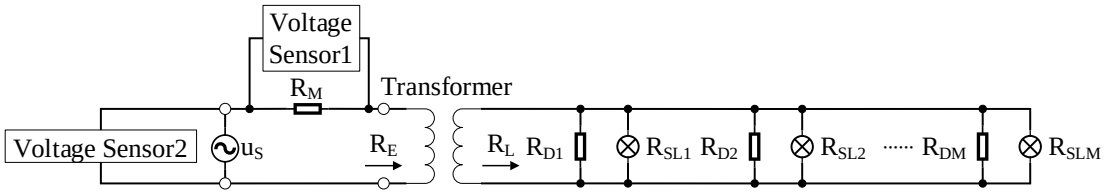

Figure 2. The frame for the resistively modulated PLCC technology in the streetlamp monitoring system

The current i_M through the primary side of the transformer can be calculated by Eq. 5:

$$i_M = \frac{u_{M1}}{R_M} \tag{5}$$

Where u_{M1} is the voltage measured by Voltage Sensor1.

The equivalent resistance R_E from the primary side to the secondary side can be obtained by Eq. 6.

$$R_E = \left(\frac{N_E}{N_L}\right)^2 R_L = \frac{u_{M(k-\frac{\phi}{F_{ADC}})}}{i_{Mk}} - R_M \tag{6}$$

Where i_{Mk} is the measured current value through the resistance at the k-th time point, F_{ADC} is the sample frequency of the ADC. The equivalent resistance on the secondary side of the transformer R_L can be calculated using Eq. 7.

$$R_L = (\ldots(((R_{SLM} \parallel R_{DM} + R_{PL}) \parallel (R_{SL(M-1)} \parallel R_{D(M-1)}) + R_{PL}) \parallel (R_{SL(M-2)} \parallel R_{D(M-2)}) + R_{PL}) \parallel \ldots + \ldots) \parallel (R_{SL1} \parallel R_{D1}) + R_{PL} \tag{7}$$

Where R_{PL} is the resistance of the power line between two adjacent street lamps.

Partial parameters of the model for the resistively modulated PLCC technology in the streetlamp monitoring system are listed in Table 1 [19–26].

Table 1. Partial parameters of the model for the resistively modulated PLCC technology in the streetlamp monitoring system

Sections	Parameters
Source Voltage	10 [kV] with deviation ±7%
The secondary voltage of the transformer	220 [V]
Distance of secondary side	2.5 [km]
Distance between 2 adjacent street lamps	25 [m]
Wire	16mm² copper wire with 1.92 [Ω/km] at 20 [℃]
Digital resistor	10 [kΩ]. Resolution is 8 [bits]. Conversion speed can be 100 [kSPS].
Street lamp: ZY904-III	The power is 100 [W]. The voltage is 220 [V].
Voltage sensor	Resolutions are 12 [bits], 14 [bits], 16 [bits], and 20 [bits] corresponding. U_{pp} corresponds to 2 [V], 1.6 [V], 2 [V], 4.096 [V].

The remaining parameters can be calculated based on the values provided in Table 1:

i. The winding ratio of the transformer is N_E/N_L = 10 kV / 220 V = 500 / 11.

ii. The number of street lamps is M = 2.5 km/25 m = 100.

iii. The resistance of each street lamp is R_{SLm} = (220 V)^2 / 100 W = 484 Ω.

iv. The resistance of each cable is R_{PL} = 25 m * 1.92 Ω/km = 0.048 Ω.

v. The measuring resistance can be calculated as follows:

To prevent u_M from exceeding the measurement range of the ADC due to changes in U_{pp}, adjustments to u_M should be made accordingly, as specified in Eq. 8.

$$\left|u_S \frac{R_M}{R_M+R_E}\right| = \left|u_S \frac{R_M}{R_M+\left(\frac{N_E}{N_L}\right)^2 R_L}\right| < U_{pp}/2 \tag{8}$$

Which leads to Eq. 9.

$$u_{Smax} \frac{R_M}{R_M+\left(\frac{N_E}{N_L}\right)^2 R_{Lmin}} < U_{pp}/2 \tag{9}$$

Where uSmax = √2 × 220 × (1 + 7%) ≈ 333V, accounting for a deviation ±7% in the source voltage. The minimum of R_L is R_{Lmin} = 1.3432Ω, considering that the minimum value of each digital resistance is R_{Dmin} = 1/2^8 * 10kΩ = 39.0625Ω. Eq. 10 can be derived from Eq. 9 to limit the R_M.

$$R_M < \frac{\left(\frac{N_E}{N_L}\right)^2 R_{Lmin} U_{pp}}{2u_{Smax} - U_{pp}} \approx \frac{2775U_{pp}}{666V - U_{pp}} \tag{10}$$

In addition, the value of R_M should be as close to the maximum as possible to improve the accuracy of the measurement.

vi. Noises

In the PLCC channel of the streetlamp monitoring system, there are five types of noises: colored background noise, narrowband noise, power frequency synchronous periodic pulse noise, power

frequency asynchronous periodic pulse noise, and random pulse noise [10, 27, 28]. The Middleton-A noise model is used to represent the characteristics of pulse noise with high amplitude and suddenness [10], which can model the noises in the PLCC channel. The noise sample points of the Middleton-A model are generated by combining background Gaussian noise and random pulse noise. The probability density function of the Middleton-A model is given by Eq. 11 according to [29].

$$f_{X_{MA}}(x) = \sum_{m_{MA}=0}^{\infty} \frac{1}{\sqrt{2\pi\sigma_{m_{MA}}^2}} \mu_{m_{MA}} e^{-\frac{|x|^2}{2\sigma_{m_{MA}}^2}} \tag{11}$$

Where,

$$\mu_{m_{MA}} = e^{-A_{MA}} \frac{(A_{MA})^{m_{MA}}}{m_{MA}} \tag{12}$$

$$\sigma_{m_{MA}}^2 = \frac{m_{MA}/A_{MA}+\Gamma_{MA}}{1+\Gamma_{MA}} \sigma^2 \tag{13}$$

Where σ^2 represents the sum of background Gaussian noise variance (σ_g^2) and pulse noise variance (σ_i^2), while the noise power ratio is denoted as $\Gamma_{MA} = \sigma_g^2/\sigma_i^2$. A_{MA} stands for the overlap index of pulse noise, with a higher A_{MA} indicating a model with more pulse noise. As A_{MA} approaches infinity, the model approximates a Gaussian distribution. Middleton-A noise sample points can be generated by Eq. 14.

$$n_{MA}=x_G+\sqrt{K_{pd}}y_I \tag{14}$$

Where x_G and y_I represent two Gaussian sequences with the same mean of 0, with variances σ_g^2 and σ_i^2/A_{MA} respectively. K_{pd} denotes Poisson distribution variables, with a mean of A_{MA}. And Eq. 15 is applicable according to [30].

$$\sigma_g^2+\sigma_i^2=1 \tag{15}$$

Table 2 presents four types of the Middleton-A noise model parameters used in [10] and [31].

Table 2. Four types of the Middleton-A noise model parameters

A_{MA}	Γ_{MA}
10	2
10	0.1
0.02	2
0.1	0.1

3.2. Design of Binary Resistive Modulation Technique

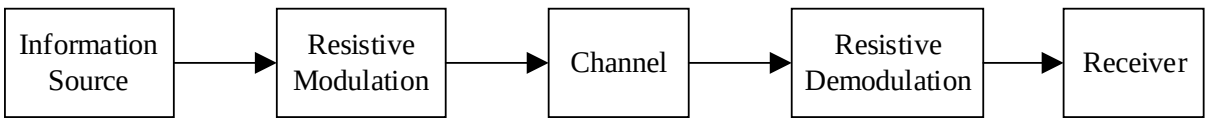

Figure 3. Resistive Communication process

As shown in Fig. 3, the communication process contains information source, resistive modulation, channel, resistive demodulation, and audience. This paper focuses on designing resistive modulation and resistive demodulation.

3.2.1. Binary Resistive Modulation.

In this paper, the high resistance (R_{high}) of the digital resistor represents binary '0', and the low resistance (R_{low}) of the digital resistor represents binary '1'. This resistance affects the current through the primary side of the transformer, as described by Eq. 5. The two types of resistance are defined as follows:

i. $R_{high} \approx 10k\Omega$.

R_{high} is set as the maximum value of the digital resistor to save more energy. While '0' is sent, the high secondary equivalent resistance $R_{Lhigh} \approx 6.14\Omega$, according to (7), and the high primary equivalent resistance $R_{Ehigh} = (N_E/N_L)^2 R_{Lhigh} \approx 12658\Omega$.

ii. $R_{low} \approx 39\Omega$

R_{low} must be less than R_{high}. So R_{low} is one case of (n / (2^8) * 10kΩ), where n = 1, 2, …, 254. While '1' is sent, the primary resistance R_{Elow} depends on the value of R_{low} and the location where the signal occurs. Fig. 4 illustrates the effect on R_{Elow} of varying the location R_{Dm} from m = 1 to m = M, with different $R_{low} = n$ / (2^8) * 10kΩ for n range from 1 to 254.

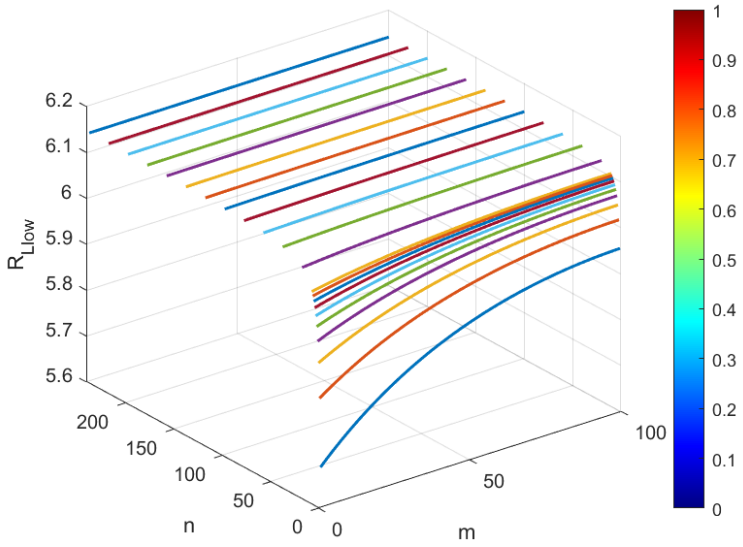

Figure 4. The effect on R_E of varied R_{Dm} with different R_{low}

From Fig. 4, It can be observed that:

i. For the same R_{Dm} with the same m, a smaller n results in a smaller R_{Elow}. Therefore, to get the smallest resistance value, n = 1 is chosen, giving R_{low} = 1/256 * 10kΩ ≈ 39Ω.

ii. For the same R_{low} with the same n, R_{Elow} increases with m. To ensure the design meets requirements in all cases, m = 100 is used in the experiments as the maximum value. At this point the low equivalent resistance on the secondary side $R_{Llow} \approx 5.8\Omega$ and the corresponding low equivalent resistance on the primary side $R_{Elow} = (N_E/N_L)^2 R_{Llow} \approx 11989\Omega$.

As discussed, the binary resistive modulation technique is used to modulate binary data as detailed in Table 3.

Table 3. Binary Resistive Modulation Technique

Binary	R_{Dm} [Ω]	R_E [Ω]
'0'	$R_{high} \approx 1\times10^4$	$R_{highE} \approx 12658$
'1'	Rlow ≈39	$R_{lowE} \leq 11989$

3.2.2. Resistive Demodulation.

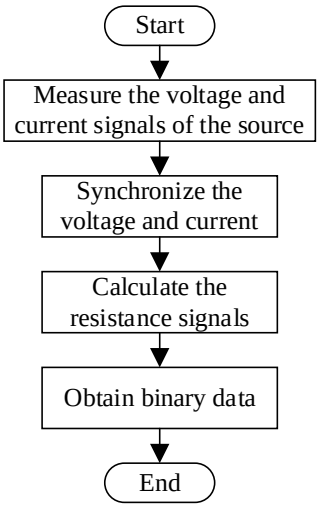

Figure 5. The process of resistive demodulation

The process of the resistive demodulation is shown in Fig. 5:

i. Measure the voltage and current of the source.

ii. Synchronize the voltage and current signals by calculating the phase difference ϕ.

iii. Acquire the resistive signals using Eq. 5.

iv. Divide the resistive signals into groups of F_{ADC}/F_{DR} points, where F_{DR} is the changing frequency of the digital resistor and F_{ADC} is the sampling frequency of the ADC. The median of each group is then taken as the value of the group, denoted R_G.

v. Obtain the binary data by comparing R_G with a threshold value: when the R_G is greater than the threshold value, binary '0' is obtained; when R_G is lower than the threshold value, binary '1' is obtained.

However, there are three issues in the resistive modulation and demodulation process caused by noise and measurement errors: i. Unbalanced probability density of measured resistance caused by noise and measurement errors. ii. Uneven distribution of errors caused by errors in the phase difference ϕ. iii. The amplification effect of source voltage errors on calculating resistance. When the current through the primary side of the transformer approaches zero, errors in resistance calculation due to source voltage inaccuracies are amplified.

i. Unbalanced probability density of measured resistance caused by noise and measurement errors.

Eq. 16 is used in the resistive PLCC system.

$$R_{EG} = \frac{u_{SG}}{i_{MG}} - R_M = \left(\frac{u_S + \Delta u_S}{u_M + \Delta u_M} - 1\right) R_M \tag{16}$$

Where R_{EG} is the measured equivalent resistance from the primary side to the secondary side, u_{SG} is the measured source voltage. i_{MG} is the measured current through R_M, Δu_S represents the error in the source voltage, and Δu_M is the error in u_M. It can be noted that Δu_M in the denominator will cause an unbalanced probability distribution of R_{EG}, which is shown in Fig. 6.

Fig. 6(a) illustrates the probability distribution of the measured high equivalent resistance R_{highEG} (when $R_{D100} = R_{high}$), whose peak deviates to the left of the ideal value R_{highE} (the ideal value shown by the dotted line). Fig. 6(b) shows the probability distribution of R_{lowEG} (when $R_{D100} = R_{low}$), whose peak deviates to the left of the ideal value R_{lowE} (the ideal value also marked by the dotted line). Fig. 6(c) combines Fig. 6(a) and Fig. 6(b), with the right dotted line representing the midpoint of R_{lowE}

and R_{highE}, and the left dotted line showing the intersection point of the two probability densities. Setting the threshold at the midpoint resulting in a total probability that can be resolved is $P_{mid} = (P_I + P_{II} + P_{III} + P_{IV} + P_{VI}) / 2$. However, setting the threshold at the intersection point yields a higher total probability $P_{inter} = (P_I + P_{II} + P_{III} + P_{IV} + P_V + P_{VI}) / 2$. Therefore, the threshold should be set at the intersection point, to achieve the highest demodulation quality.

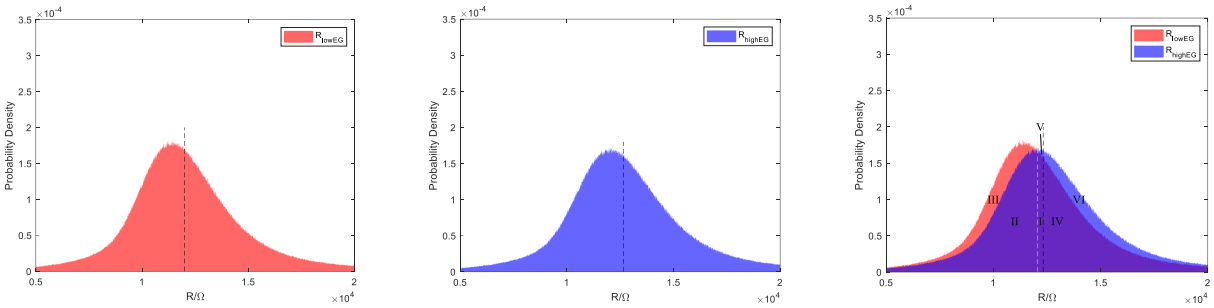

(a) (b) (c)

Figure 6. Unbalanced probability distribution of R_{EG} when R_{D100} = (a) R_{low}, (b)R_{high}, and (c) R_{low} and R_{high}

Fig. 7 illustrates the impact of different thresholds on the Bit Error Ratio (BER) in two cases: $u_S > 0$ and $u_S < 0$, the dotted line represents the midpoint of R_{Ehigh} and R_{Elow}. i. When $u_S > 0$, the threshold that results in the lowest BER is to the right of the midpoint. ii. When $u_S < 0$, the threshold that results in the lowest BER is to the left of the midpoint.

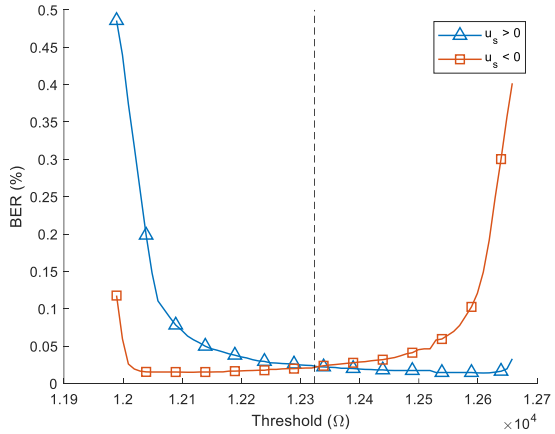

Figure 7. Relationship between the BER and thresholds

ii. Uneven distribution of errors caused by errors in the phase difference ϕ.

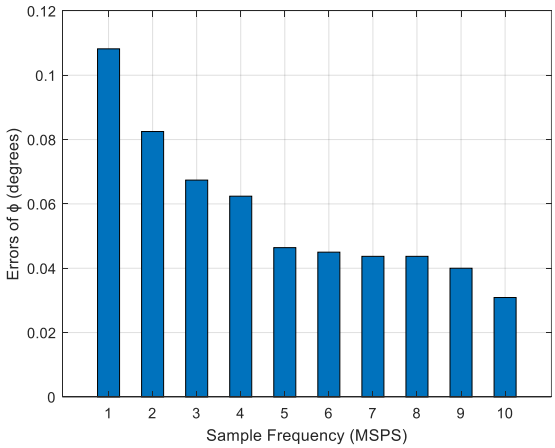

Figure 8. The relationship between errors in ϕ and the sample frequency of ADC

As shown in Fig. 8, the error in ϕ caused by noise and measurement errors is related to the sample frequency of ADC. As sample frequency increases, the error in ϕ decreases, which in turn affects communication quality. As shown in Fig. 9, the BER decreases as the sampling frequency of ADC increases.

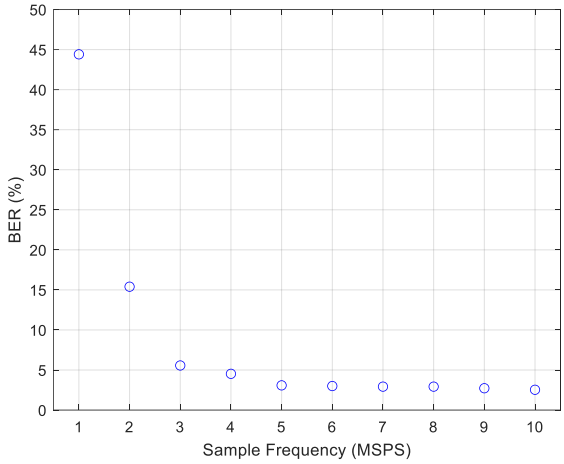

Figure 9. Relationship between BER and sample frequency

According to Eq. 17, a given error ($d\phi$) in ϕ will result in varying errors (du_S) in u_S depending on the time (t) at which the error occurs.

$$\frac{du_S}{d\phi} = \frac{dsin(\omega t+\phi_{uS})}{d\phi} = \frac{dsin(\omega t+\phi_{uM}+\phi)}{d\phi} = \cos(\omega t + \phi_{uM} + \phi) \tag{17}$$

Where ω is the angular frequency, ϕ_{uM} is the initial phase of u_M, and ϕ_{uS} is the initial phase of u_S.

To address the issue, two approaches can be applied:

(a) Increase the sampling frequency of ADC to reduce errors in ϕ.

(b) Avoid the regions where the error in u_S is highly sensitive to the error in ϕ.

iii. Amplification effect of source voltage errors on calculating resistance.

As shown in Eq. 18, the error (ΔR_E) in R_E caused by the error (Δu_S) of u_S increases as the absolute of current i decreases. Specifically, as i approaches zero, ΔR_E is amplified significantly.

$$\Delta R_E = \frac{\Delta u_S}{i} \tag{18}$$

To address the issue, two approaches can be applied:

(a) Improve the ADC resolution to reduce the measurement errors.

(b) Avoid regions where the current approaches zero.

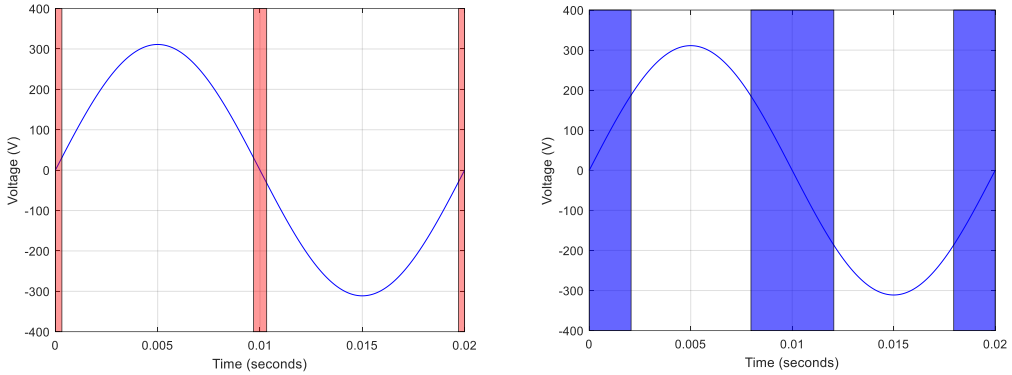

(a) (b)

Figure 10. Dead zones where (a) current approaches zero and (b) where the error in u_S is highly sensitive to the error in ϕ

Considering the last two issues, the regions to avoid are shown in Fig. 10. Fig. 10(a) shows the regions where the current approaches zero, while Fig. 10(b) shows the regions where the error of u_S is highly sensitive to the error in ϕ. The two types of regions are referred to as "dead zones" in this paper. The actual communication should be limited to the regions near the peaks. The proportion of the limited communication regions to the total communication time is termed the "time availability of communication" (P_C).

$$P_C = \frac{T_C}{T} \times 100\% \tag{19}$$

Where T_C is the time available for communication within one period, and T is the total period.

Based on the previous discussion, two approaches can be used to improve communication quality: i. Increase the ADC resolution, to reduce measurement errors. ii. Decrease the time availability of communication (P_C) to avoid dead zones.

In Fig. 11, R_m represents the resistance measurement result, R_{Ehigh} represents the high level of the equivalent resistance R_E from the primary side of the transformer to the secondary side, and R_{Elow} represents the low level of R_E. The horizontal axis shows the resistance value, and the vertical axis divides the whole plane into left and right parts by the midpoint between R_{Ehigh} and R_{Elow}. Observations include: i. In Fig. 11(a), with a 12-bit ADC resolution, the mapping appears more cluttered, with points overlapping and making them difficult to distinguish. ii. In Fig. 11(b), with a 20-bit ADC resolution, the mapping is clearer while the points are more distinctly separated into left and right groups, improving distinguishability.

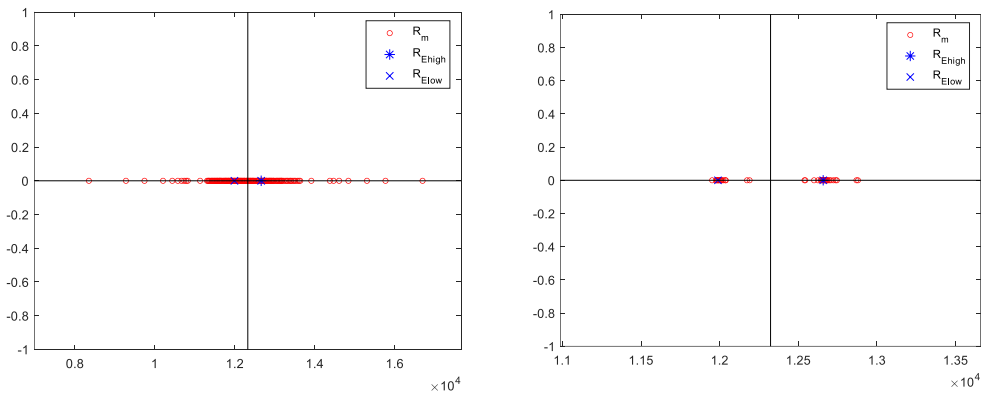

(a) (b)

Figure 11. Constellation Diagram with ADC resolution (a) 12 bits and (b) 20 bits

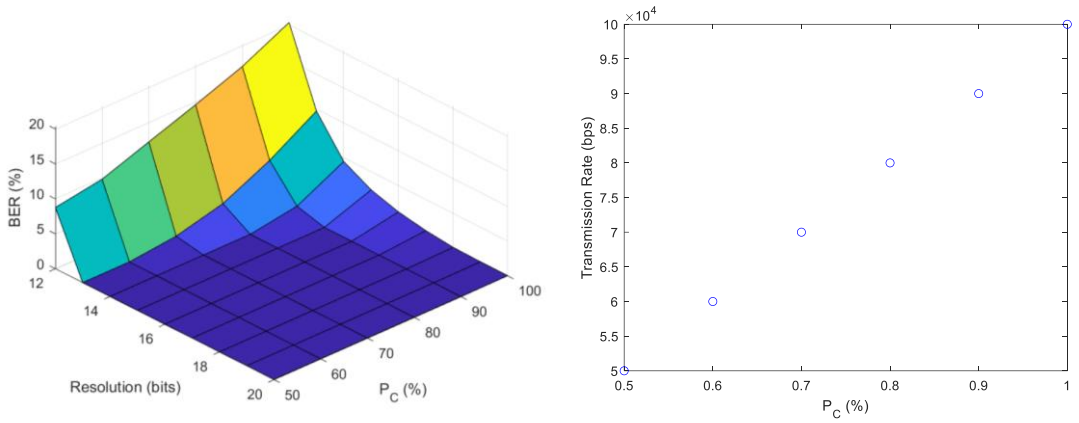

(a) (b)

Figure 12. Influence on (a) BER with ADC resolution and P_C (b) Transmission Rate with P_C

Fig. 12(a) shows that the BER decreases with both increasing ADC resolution and decreasing P_C; ii. Fig. 12(b) shows that the transmission rate decreases as P_C increases.

3.3. System Performance

Based on the analysis above, to balance BER and transmission rate, the communication system is configured with a time availability of communication P_C set as 90% and the MAX11905 ADC is selected, featuring a 20-bit resolution, a U_{pp} of ±3.6V, and a sample frequency of 1.6 MSPS.

Testing the designed binary resistive modulated PLCC system model using the specified parameters yielded the results shown in Table 4. The communication rate can reach 90 kbps, and BER is 0.1%, which is acceptable for the intended applications. Additionally, the system can transmit signals across the transformer, where the resistive signals are enhanced by 46 dB. And it allows the system to transmit signals over 2.5 km as the resistive signal attenuation in the power line is less than 1 dB/km.

Table 4. The performance of the designed resistive modulated PLCC technology in the streetlamp monitoring system

Metrics	Values
Resistive signal attenuation in this power line	< 1 dB/km
Resistive signal enhancement in the transformer	46 dB
BER	0.1%
Communication rate	90 kbps
Communication distance	2.5 km

4. SUMMARY

By comparing different techniques and parameters, this paper establishes a model of the PLCC system with binary resistive modulation for streetlamp monitoring. Experimental results demonstrate two advantages of introducing the resistive modulation technique: i. The system reduces the signal attenuation in the power line, allowing for long-distance communication; ii. The system enhances resistive signals as they pass across the transformer, enabling transmission across transformers.

REFERENCES

[1] Tian, G. R., “Design of Intelligent Street Lamp Control System Based on LoRa Technology,” Master's thesis, Beijing Institute of Petrochemical Engineering, 2021. Beijing, China. doi: 10.27849/d.cnki.gshyj.2021.000037.

[2] Tung, N. T., Phong, N. H., Huy, T. L. D., Huy, N. M., Tuyen, N. D., and Phuong, L. M., "Development and performance analysis of intelligent street lighting for smart cities using LoRa Wan," Engineering and Technology, vol. 2, no. 3, pp. 193-206, 2020.

[3] Li, N., "The LED Power Supply with the Integration of Driver and Management Based on the Power Line Communication," Master's thesis, North China Electric Power University, 2017. Beijing, China. Available: https://kns-cnki-net-443.webvpn.axhu.edu.cn/KCMS/detail/detail.aspx?dbname=CMFD201901&filename=1018276884.nh

[4] Zhang, C. Y., "Research on LED Control Algorithm Based on Low Voltage Power Line Carrier Communication," Master's thesis, South China University of Technology, 2020. Guangzhou, Guangdong, China. Available: https://kns-cnki-net-443.webvpn.axhu.edu.cn/KCMS/detail/detail.aspx?dbname=CMFD202101&filename=1021546568.nh

[5] He, H. C., "Intelligent street lamp management system based on NB-IoT," Master's thesis, Fuzhou University, 2019. Fuzhou, Fujian, China. Available: https://kns-cnki-net-443.webvpn.axhu.edu.cn/KCMS/detail/detail.aspx?dbname=CMFD202102&filename=1021503643.nh

[6] Zhang, N., "Design and Implementation of Intelligent Street Light Control System Based on NB-IOT," Master's thesis, Lanzhou University, 2019. Lanzhou, Gansu, China. Available: https://kns.cnki.net/KCMS/detail/detail.aspx?dbname=CMFD202001& filename=1020603114.nh

[7] Huang, Z. C., "Application of Wireless Sensor Network Based on 6Lo WPAN in Smart Lighting," Master's thesis, South China University of Technology, 2015. Guangzhou, Guangdong. https://kns.cnki.net/KCMS/detail/detail.aspx?dbname=CMFD201601& filename=1015989647.nh

[8] Xue, Y. S., "Plug-and-play Automatic Identification Technology for Smart Home Based on Electric Power," Master's thesis, North China Electric Power University, 2020. Beijing, China. Available: https://kns-cnki-net-443.webvpn.axhu.edu.cn/KCMS/ detail/detail.aspx?dbname=CMFD202101&filename=1021012138.nh

[9] Ahiadormey, R. K., Anokye, P., Jo, H. S., and Lee, K. J., "Performance analysis of two-way relaying in cooperative power line communications," IEEE Access, vol. 7, pp. 97264-97280, 2019.

[10] Lin, J. X., "Research on Key Technologies of Broadband Power Line Communication System Based on OFDM," Master's thesis, Zhejiang University, 2021. Hangzhou, Zhejiang, China. Available: https://kns-cnki-net-443.webvpn.axhu.edu.cn/KCMS/detail/ detail.aspx?dbname=CMFD202201&filename=1021789892.nh

[11] Kang, H., "Research on High Reliability Channel Coding of MIMO-PLC," Master's thesis, North China Electric Power University, 2021. Beijing, China. Available: https://kns-cnki-net-443.webvpn.axhu.edu.cn/KCMS/detail/detail.aspx? dbname=CMFD202201 &filename=1021885079.nh

[12] Shen, D., Cheng, W. B., Wang, X. F., and Yang, J. C., "Accurate control of intelligent streetlamp based on carrier communication," Journal of Lighting Engineering, vol. 04, pp. 35-39, 2019. doi: CNKI:SUN:ZMGX.0.2019-04-014.

[13] Yue, J. Q., Wang, L. J., Lu, Z. D., and Tang, D. Q., "Streetlight Monitoring System Based on the Power Carrier Communication Technology," Information and Communication, vol. 12, pp. 164-165, 2018. doi: CNKI:SUN:HBYD.0.2018-12-072.

[14] Zhao, X. D., "Research on Network and Routing Control Technology of Smart Street Light Based on IPv6," Master's thesis, Chongqing University of Posts and Telecommunications, 2019. Chongqing, China. Available: https://kns-cnki-net-443.webvpn. axhu.edu.cn/KCMS/detail/detail.aspx?dbname=CMFD202001&filename=1019643630.nh

[15] Zhang, Y. J., Li, D., and Guo, X. Y., "Design of the Streetlamp Lighting System of the Power Carrier Based on the Internet+," Electronic Devices, vol. 40, no. 3 pp. 651-655, 2017.

[16] ysics Teaching. 40(07), pp. 69-71.

[17] Qiu, G. Y. & Luo X. J., et al. "Circuit (5th Edition)," in Higher Education Press, 2006.

[18] Yu, X., "Comparative Analysis of Denoising Performance between Traditional Filter and Adaptive Filter," Shanxi Electronic Technology, vol. 03, pp. 16-18, 2021.

[19] Ministry of Housing and Urban-Rural Development of the People's Republic of China, "Standard for lighting design of urban road (CJJ 45-2015)," China Standards Press, 2015. Beijing, China. Available: https://www.doc88.com/p-7418489772281.html

[20] General Administration of Quality Supervision, Inspection and Quarantine of the People's Republic of China, and Standardization Administration of China, "Power Quality Supply Voltage Deviation (GB/T 12325-2008)," China Standards Press, 2008. Beijing, China. Available: https://www.doc88.com/p-7824749575406.html

[21] Maxim Integrated, "MAX5480: 8-Bit Parallel DAC in QSOP-16 Package Data Sheet (Rev.0)," California, USA. Available: https://www.analog.com/en/products/max5480.html#documentation

[22] Shanghai Yaming Lighting Co., Ltd., "ZY904-III," Shanghai, China. Available: https://yaming.inesa.com/shinesa_ymzm_jgdj/2023-05-12/Detail_167356.htm

[23] Analog Devices, “AD9234: 12-Bit, 1 GSPS/500 MSPS JESD204B, Dual Analog-to-Digital Converter Data Sheet (Rev.B),” norwood, Massachusetts, USA. Available: https://www.analog.com/media/en/technical-documentation/data-sheets/ad9234.pdf

[24] Analog Devices, “AD9680: 14-Bit, 1.25 GSPS/1 GSPS/820 MSPS/500 MSPS JESD204B, Dual Analog-to-Digital Converter Data Sheet (Rev.E),” norwood, Massachusetts, USA. Available: https://www.analog.com/media/en/technical-documentation/data-sheets/AD9680.pdf

[25] Texas Instruments, “ADS54J60 Dual-Channel, 16-Bit, 1.0-GSPS Analog-to-Digital Converter datasheet (Rev. D),” norwood, Massachusetts, USA. Available: https://www.ti.com/lit/ds/symlink/ads54j60.pdf?ts=1721581264624&ref_url=http%253A%252F%252Fti.com%252Ftool%252FTIDA-00822

[26] Analog Devices, “MAX11905: 20-Bit, 1.6Msps, Low-Power, Fully Differential SAR ADC Data Sheet (Rev.4),” norwood, Massachusetts, USA. Available: https://www.analog.com/media/en/technical-documentation/data-sheets/MAX11905.pdf

[27] Shao, T. Y., “Research on Noise and Characteristics of Low Voltage Power Line Channel,” Master's thesis, Harbin Institute of Technology, 2014. Harbin, Heilongjiang, China. Available: https://kns-cnki-net-443.webvpn.axhu.edu.cn/ KCMS/detail/detail. aspx?dbname=CMFD201501&filename=1014082121.nh

[28] Chen, Y. W., Xu, B., Hao, J. H., & Zhang, Z. B., “Modeling and Simulation of Power Line Communication System Based on OFDM Technology,” Foreign Electronic Measurement Technology, vol. 02, pp. 21-26, 2015. doi: 10.19652/j.carolcarrollnki. femt.2015.02.002

[29] Wang, J. J., “Research on Noise Characteristics and Channel Estimation Method of Low Voltage Power Line Communication,” Master's thesis, Chongqing University of Posts and Telecommunications, 2020. Chongqing, China. Available: https://kns-cnki-net-443.webvpn.axhu.edu.cn/KCMS/detail/detail.aspx?dbname=CMFD202101&filename=1020417182.nh

[30] Cortés, J. A., Sanz, A., Estopinán, P., & García, J. I., “On the suitability of the Middleton class A noise model for narrowband PLC,” in 2016 International Symposium on Power Line Communications and its Applications (ISPLC), 2016, pp. 58-63. IEEE.

[31] Wang, W., “Research on Key Technologies of Low Voltage Power Line Carrier Communication,” Master's thesis, China University of Mining, 2021. Beijing, China. Available: https://kns-cnki-net-443.webvpn.axhu.edu.cn/KCMS/detail/detail.aspx?dbname=CMFD202201&filename=1021775204.nh